Triplet-Induced Singlet Oxygen Photobleaches Near Infrared Dye-Sensitized Upconversion Nanosystems

Xindong Wang[1,2,3&], Chang Jiang[1&], Zeming Wang[2], Bruce E. Cohen[2,4], Emory M. Chan[2], and Guanying Chen[1]*

[1] MIIT Key Laboratory of Critical Materials Technology for New Energy Conversion and Storage, School of Chemistry and Chemical Engineering & Key Laboratory of Micro-systems and Micro-structures, Ministry of Education, Harbin Institute of Technology, Harbin, 150001, China

[2] The Molecular Foundry, Lawrence Berkeley National Laboratory, Berkeley, CA 94720, United States

[3] Institute of Flexible Electronics Technology of THU, Zhejiang Jiaxing & Key Laboratory of Flexible Electronics based Intelligent Sensing and Advanced Manufacturing Technology, Jiaxing, 314006, China

[4] Division of Molecular Biophysics & Integrated Bioimaging, Lawrence Berkeley National Laboratory, Berkeley, CA 94720, United States

KEYWORDS: Upconversion nanoparticles, near-infrared dye, triplet state, photobleaching, singlet oxygen

ABSTRACT: The rapid photobleaching of near-infrared (NIR) dye-sensitized upconversion nanosystems is one of the crucial problems that has blocked their technological applications. Uncovering the photophysical and photochemical pathways of NIR dyes would help to elucidate the photobleaching mechanism and thereby improve the photostability of the system. Here we investigate the triplet dynamics of NIR dyes and their interaction with triplet oxygen in the typically investigated IR806-sensitized upconversion nanoparticles (UCNPs) nanosystem. Low-temperature fluorescence at 77 K provides direct proof of the generation of

singlet oxygen ($^1O_2$) under 808 nm laser irradiation. Mass spectrometry indicates that all three double bonds in the structure of IR806 can be broken in the photochemical process. Coupling IR806 to the surface of UCNPs can accelerate its triplet dynamics, thus producing more $^1O_2$ to photocleave IR806. Importantly, we find that addition of β-carotene can scavenge the generated $^1O_2$, thereby providing a simple method to effectively inhibit photobleaching.

Introduction

Lanthanide-doped upconversion nanoparticles (UCNPs) are able to emit bright ultraviolet or visible luminescence under moderate near-infrared (NIR) light irradiance (~0.1-10^2 W/cm^2)[1]. Due to the advantages of large anti-Stokes shift, tunable spectra spanning from ultraviolet to NIR, long lifetimes of up to milliseconds, and near-zero photobleaching, UCNPs are attractive for applications in bioimaging[2, 3], biological and chemical sensing[4, 5], light-controlled drug release[6], optogenetics[7], and anti-counterfeiting[8]. A laser is typically required to excite UCNPs because of the narrow and weak absorption associated with the nature of the 4*f*-4*f* electronic transitions of lanthanide ions, largely restricting the use of UCNPs in portable devices.

Various methods have been developed to enhance the absorption capacity of UCNPs, such as introducing NIR organic dyes as sensitizers[9, 10], plasmonic-induced upconversion enhancement[11, 12], and co-doping sensitizer ions with a larger absorption cross-section[13]. Among these attempts, sensitization with NIR dyes has the advantages of ease of operation, broad absorption spectra (10 times broader FWHM than that of lanthanide absorption) and high absorption cross-section (1000-10000 times higher than those of lanthanide ions)[14], significantly increasing upconversion brightness by up to 33000-fold[15]. However, these reported dye-sensitized upconversion nanosystems suffer from severe photobleaching when exposed to oxygen[15].

Photobleaching can be minimized by encapsulating dye-sensitized upconversion nanosystems into polymers[16] or by performing experiments in inert atmosphere, but limited impact to fuel applications. Since UCNPs are highly stable[1] even under laser power densities up to 10^7 W/cm^2, photobleaching typically originates from the NIR dye or the interaction between NIR dye and UCNPs. It is generally believed that the

NIR dyes are damaged by singlet oxygen ($^1O_2$), which is produced by the energy transfer (ET) from the triplet state of NIR dye to triplet oxygen[17]. While there is indirect proof of the generation of $^1O_2$ during excitation of the NIR dye[18, 19], direct proof[20-22] is lacking in the dye-sensitized upconvesion nanosystems due to the intrinsically low quantum yield (ca. 10^{-7}) of $^1O_2$ emission[23]. In dye-sensitized nanosystems, lanthanide ions were also found to promote intersystem crossing in excited NIR dyes (IR806), relaxing from their singlet to its triplet excited state, and thus improve the ET efficiency from IR806 to UCNPs[15]. However, the ET pathways to triplet oxygen, inevitable in real applications, have not yet been considered. Hence, the dynamics of reactive oxygen species (ROS) such as $^1O_2$ and possible superoxide anion ($\cdot O_2^-$)[22, 24] in the presence of free NIR dyes and UCNPs-conjoined ones, demand investigations.

Herein, we studied the photophysical and photochemical pathways of IR806 in IR806-sensitized $NaYF_4$:Yb^{3+}, Er^{3+} UCNPs nanosystems, which confirm the critical effect of triplet oxygen in photobleaching. By using the low-temperature fluorescence detection at 77 K, we directly observed the generation of $^1O_2$ in the free IR806 and IR806-sensitized $NaYF_4$:Yb^{3+},Er^{3+} UCNPs nanosystems. Further, we verified that the triplet dynamics of IR806 dyes would be accelerated after their coordination to the surface of UCNPs. To scavenge the generated $^1O_2$, we provided a simple and universal method to improve the photostability of dye-sensitized nanosystems via β-carotene (Car) addition.

Results

To begin, we synthesized IR806, the first and also the most widely used dye to be studied in dye-sensitized upconversion nanosystems[9], and verified the product through its absorption wavelength maximum at 806 nm in chloroform (Figure 1a) and

^{1}H NMR (SI Methods). In air, the color of IR806 changes from light green to maple after being irradiated by an 808 nm laser. This observation is supported by a dramatic 98% drop in the dye absorption intensity at 806 nm (Figure 1a). By comparing the photostability of IR806 exposed to different concentrations of O_2, we concluded that photobleaching is positively correlated to O_2 concentration (Supporting Information, Figure S1). To explore the possible mechanism of photobleaching, density functional theory (DFT) calculations were performed with the RB3LYP exchange functional employing 6-31G basis sets using a suite of Gaussian 09 programs (Figure 1b). Calculations show that the electrons on the highest occupied molecular orbital (HOMO) and the lowest unoccupied molecular orbital (LUMO) of IR806 are mainly located at the carboxyl group and the conjugated carbon chain, suggesting the conjugated carbon chain is prone to react with strongly electrophilic molecules such as $^1O_2$.

Low-temperature fluorescence at 77 K and electron spin resonance (ESR) spectra were used to verify the composition of the ROS involved in the photophysical process. Unlike additive-assisted methods that indirectly probe the presence of singlet oxygen using $^1O_2$-reactive agents, direct measurement of $^1O_2$ emission provides unambiguous, real-time information, less susceptible to interference from other ROS. Measurements were acquired at low temperature to increase the signal-to-background ratio of the $^1O_2$ emission. The fluorescence peak at 1275 nm (Figure 1c) is attributed to the emission of $^1O_2$ [25], directly proving the generation of $^1O_2$. Moreover, the generated $\cdot O_2^-$ via electron transfer may also participate in the photobleaching process[22, 24], whereas it has not been considered in the previous studies of dye-sensitized nanosystems. We performed ESR detection in the irradiated IR806 solution using 2,2,6,6-tetramethylpiperidine (TEMP) and 5,5-dimethyl-1-pyrroline-N-oxide

(DMPO) as capture agents for $^1O_2$ and $\cdot O_2^-$. The distinctive three peaks in the ESR spectra in Figure 1d confirm the production of $^1O_2$, while the low background signal does not show any evidence of $\cdot O_2^-$ (Figure 1e). To further support the reaction mechanism calculated by DFT, we analyzed the photooxidative products of IR806 by mass spectrometry, which provides compelling proof[17], and found two major cleaved products (Figure 1f). We hypothesize that these two major products are caused by oxidation of the double bonds on the conjugated carbon chain, revealing all the three double bonds (circled in red in Figure 1f) of IR806 can be ruptured in the photochemical process.

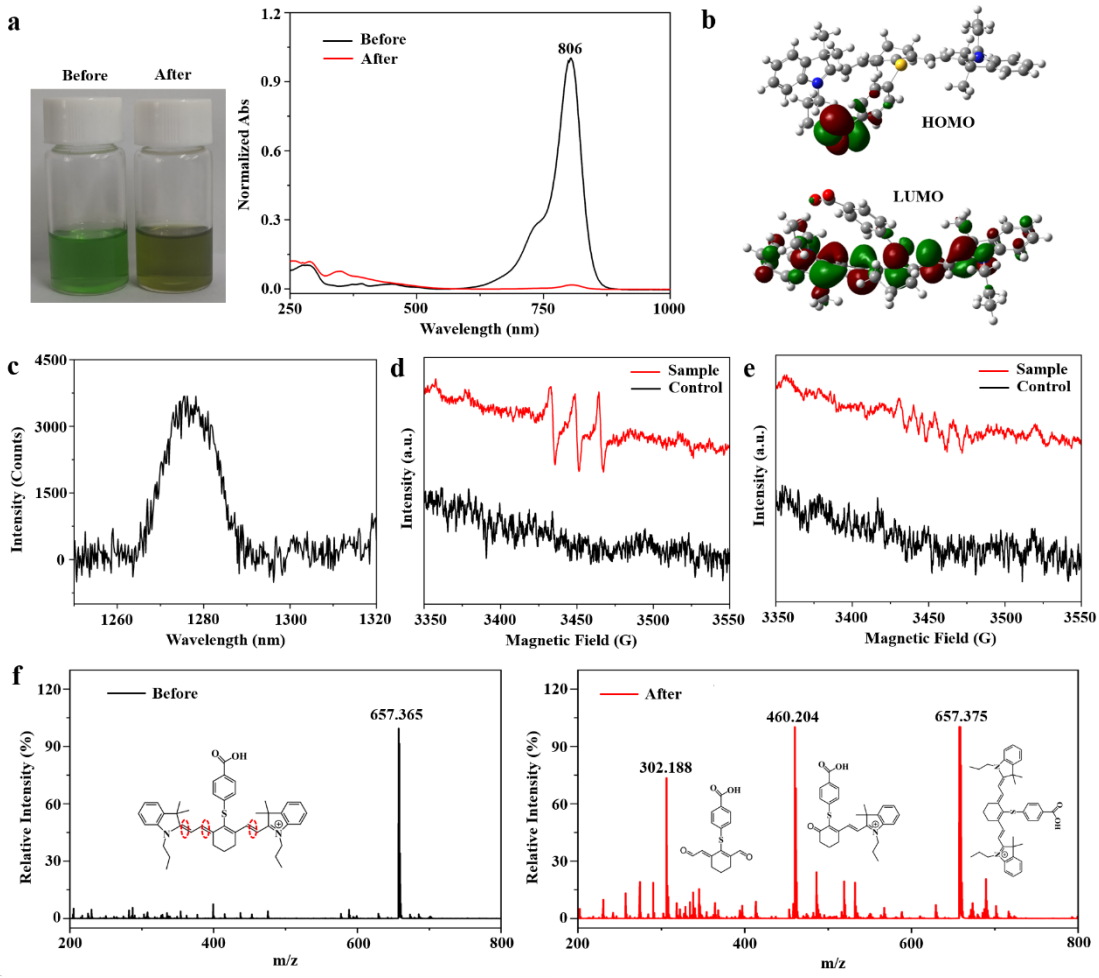

Figure 1. Photooxidative cleavage of IR806. (a) Photographs and absorption spectra of IR806 before and after photobleaching. (b) HOMO and LUMO diagrams of IR806. (c) Emission spectrum of IR806 irradiated by 808 nm laser at 77 K. (d) ESR detection of $^1O_2$ trapped by TEMP. (e) ESR detection of $\cdot O_2^-$ trapped by DMPO. Sample and Control refer to IR806 irradiated and not irradiated by 808 nm laser, respectively. (f) Mass spectrometry of IR806 before and after photobleaching.

To study the nature of dye-sensitized nanosystems, we synthesized IR806-sensitized $NaYF_4$:Yb^{3+},Er^{3+} nanocrystals as a research model. In these structures (Figure 2a, 2b), incident 808 nm photons excite IR806 molecules, which can then relax radiatively or via nonradiative pathways including ET to Yb^{3+} and vibrational/rotational relaxation. Energy transferred to Yb^{3+} can give rise to energy transfer upconversion and luminescence from Er^{3+} (and Yb^{3+}). Transmission electron microscopy (TEM) of synthesized UCNPs shows highly uniform hexagonal shapes with a mean size of 28.0 nm (Figure 2c). In the fabricated nanosystems, IR806 exhibits light absorption from 700 to 850 nm, peaking at 806 nm (Figure 2d). Thus, the commercially available 808 nm laser was selected as the excitation source. The fluorescence spectrum of IR806 upon the irradiation of 808 nm laser is accessible up to 1000 nm, which overlaps with the absorption spectrum of Yb^{3+} doped in the UCNPs, indicating a feasible ET pathway from IR806 to Yb^{3+}. Under 808 nm excitation, the nanosystems show luminescence of Yb^{3+} and Er^{3+} (Figure 2e, 2f), verifying energy transfer between IR806 and UCNPs. The optimal molar ratio of UCNPs and IR806 molecules is estimated to be 1:88 (Supporting Information, Figure S2), at which the upconversion luminescence is enhanced by 52-fold via the IR806-sensitization (Figure 2f).

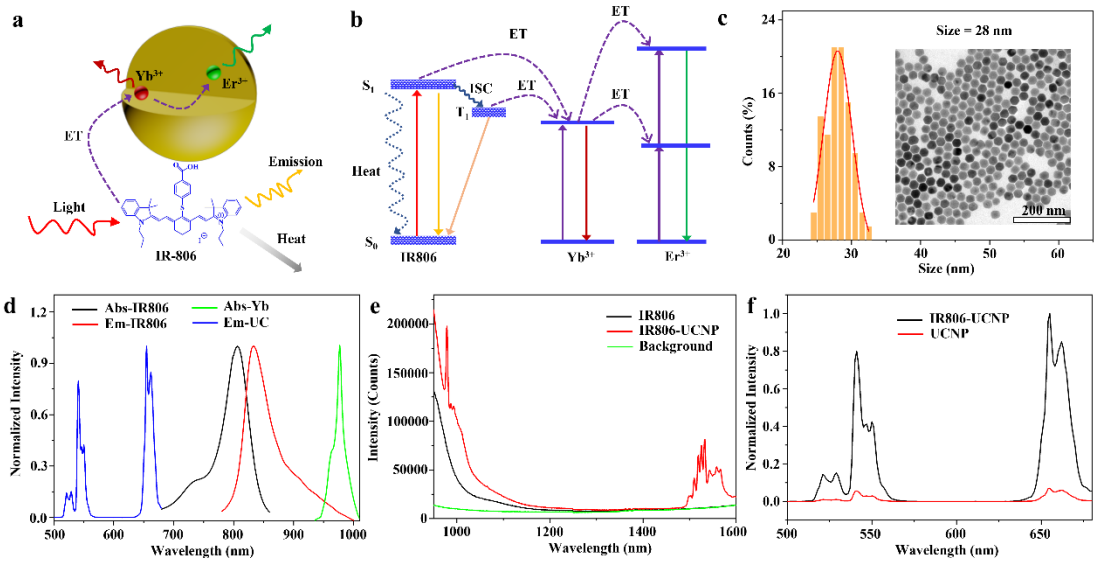

Figure 2. Fabrication of IR806-sensitized upconversion nanosystems. (a) and (b) Scheme and ET diagram of IR806-sensitized $NaYF_4$:Yb^{3+},Er^{3+} UCNPs. (c) TEM and size distribution of the synthesized UCNPs. (d) Absorption spectra of IR806 and UCNPs (Abs-IR806 and Abs-Yb), fluorescence spectrum of IR806 (Em-IR806), and upconversion spectrum of UCNPs (Em-UC). (e) Emission spectra of IR806-sensitized nanosystems (IR806-UCNP), IR806 (IR806), and blank solvent (Background) upon the irradiation of 808 nm laser. (f) Upconversion spectra of IR806-sensitized nanosystems under 808 nm laser irradiation (IR806-UCNP) and UCNPs under 980 nm laser irradiation (UCNP) with the same power density of 1.82 W/cm^2.

We investigated the luminescence dynamics of free IR806 and UCNPs-anchored ones in chloroform to reveal the influence of UCNPs on the triplet state of organic dyes[26]. As shown in Figure 3a, O_2 can be converted to $^1O_2$ in the presence of dye-sensitized UCNPs via two possible mechanisms: (1) Absorbed energy is transferred from the triplet state of IR806 to O_2. (2) The excited Yb^{3+} ions transfer energy directly to O_2 to generate $^1O_2$ [27]. Upon 980 nm irradiation of UCNPs, there is no measurable $^1O_2$ generation even after continuous excitation for 10 min (Supporting Information,

Figure S3), indicating that $^1O_2$ cannot be produced by UCNPs. Hence, the generation of $^1O_2$ is directly related to IR806 in our fabricated nanosystems. Under 808 nm laser irradiation, the emission of free IR806 and upconversion luminescence of the nanosystems both show decreasing intensities with prolonged time, and the nanosystems show more luminescence loss (75%) than free IR806 (20%) (Figure 3b). Fluorescence measurements at 77 K were used to compare the relative content of $^1O_2$ produced by free IR806 and IR806-sensitized nanosystems (the same amount of IR806 was used in both systems in Figure 3c). The $^1O_2$ content produced by the nanosystems is 5-fold more than the free IR806, revealing that the triplet dynamics of IR806 are accelerated after being coordinated on the surface of UCNPs. In addition, 1,3-diphenylisobenzofuran (DPBF) was used to further support the different amounts of $^1O_2$ production (Supporting Information, Figure S4).

To improve the photostability of IR806 and IR806-sensitized nanosystems, we choose to use reagents to scavenge $^1O_2$.[23,29] We choose β-carotene as scavenger because it is a well-established $^1O_2$ quencher in the thylakoid membrane[28,29], and can be easily incorporated in both organic and aqueous phase dye-sensitized upconversion systems. The Car itself exhibited high stability under 808 nm laser irradiation (Supporting Information, Figure S5). The large number of unsaturated double bonds in the structure of Car, can scavenge $^1O_2$ by both physical and chemical quenching pathways (Figure 3d). The physical quenching pathway provides a $^1O_2$ clearance rate of $1.5\sim2.3\times10^{10}$ M^{-1} s^{-1}, which is comparable to the diffusion rate of $^1O_2$ in solution[30]. Although the chemical quenching pathway is not as efficient as the physical one, it still exists in the system, as evidenced by structural damage (Supporting Information, Figure S6). After irradiated for 30 min at a molar ratio of 1:1, the fluorescence of IR806 decreased by 20%, while the Car-protected IR806 system only decreases by

6%, illustrating the effectiveness of the Car (Figure 3e). After irradiated for 30 min at different molar ratios of 1:0, 1:1000, and 1:5000 (IR806-sensitized UCNPs:Car), the nanosystems without Car decreased by 75%, while the Car-protected nanosystems decreased by only 60% and 42%, further demonstrating the scavenging capacity of $^1O_2$ in the IR806-sensitized UCNPs nanosystems. An increase in the Car amounts can increase the collision probability between Car and $^1O_2$, thus protecting IR806 from photobleaching more efficiently. However, the enhanced Car amounts reduce the upconversion brightness due to the reabsorption or scattering of upconversion emission by Car (Supporting Information, Figure S7), emphasizing the need to develop $^1O_2$ scavengers with lower spectral overlap. However, the downconversion luminescence of Er^{3+} is insensitive to the Car concentration, which is beneficial given the need for high Car amounts.

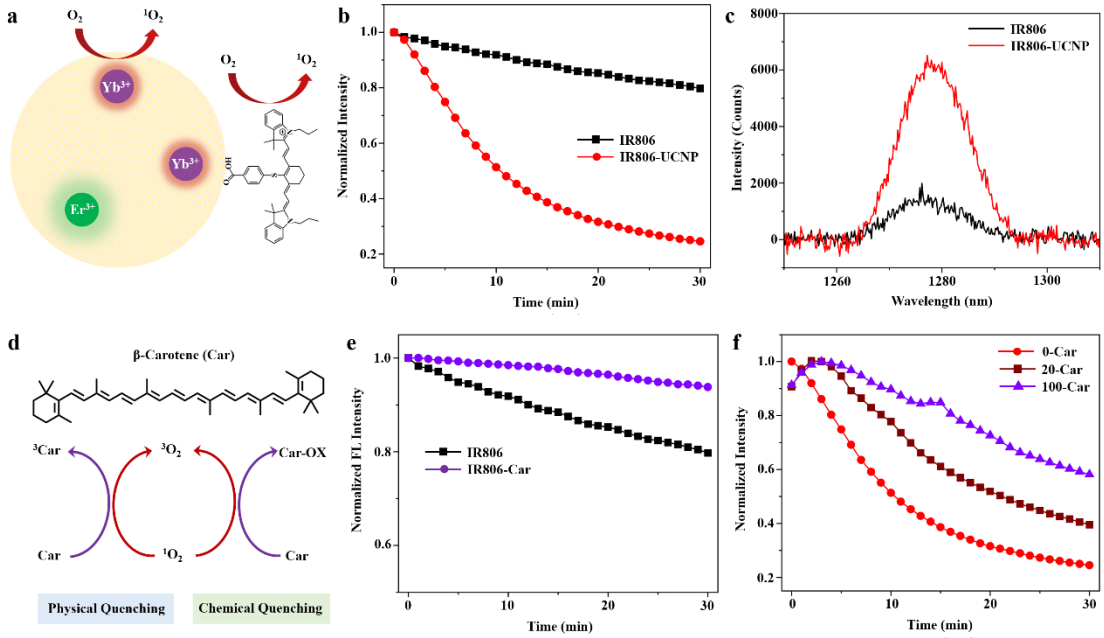

Figure 3. Photostability of IR806 and IR806-sensitized nanosystems in chloroform. (a) Scheme of possible pathways to produce $^1O_2$ in the nanosystems. (b) Normalized luminescent intensity kinetics of IR806 and nanosystems (IR806-UCNP) upon 808

nm laser irradiation. (c) Produced $^1O_2$ of IR806 and nanosystems (IR806-UCNP) upon 808 nm laser irradiation; IR806 dosages in the two systems are the same. (d) Chemical structure of Car and $^1O_2$ quenching pathways. (e) Normalized fluorescent intensity kinetics of IR806 mixed with or without Car under 808 nm laser irradiation with a power density of 1.82 W/cm^2. (f) Normalized luminescent intensity kinetics of nanosystems mixed with 0, 20, and 100 μL Car upon the irradiation of 808 nm laser with a power density of 1.82 W/cm^2. Normalization was performed to the integrated intensity of the green upconversion emission at 540 nm.

After the investigation in organic phase, we further studied the improved photostability of Car-protected IR806-sensitized nanosystems in water phase. The lipid DSPE-PEG(2000)-COOH was used to convert the IR806-sensitized nanosystems from hydrophobic to water-soluble, which was shown in Figure 4a (No Car). Due to its conjugated carbon chain structure, Car can be inserted into the DSPE-PEG(2000)-COOH layers on the surface of UCNPs, showing the nanosystem as an orange transparent solution (Figure 4a, with Car). Under 808 nm laser irradiation, the upconversion luminescence of the nanosystems with Car protection does show improved stability as compared to the one without Car (Figure 4b). The synthesized IR806-sensitized nanosystems with or without Car were then used to stain B16-F10 cells and subsequently imaged by widefield microscopy. The stained cells exhibit normal and regular cellular morphology (brightfield image), and apparent upconversion luminescence cellular imaging can be seen at laser-irradiated locations (Figure 4c). As expected, cellular fluorescence imaging showed improved stability in aqueous Car-protected nanosystem as compared to non-protected one (Figure 4d, and Supporting Information, Figure S8). Hence, we conclude that the Car-protected

strategy can be used to improve the applicability of dye-sensitized nanosystems both in organic and water-soluble solutions.

Figure 4. Photostability of IR806-sensitized nanosystems with or without Car protection in the water phase. (a) Photographs of the IR806-sensitized nanosystems in water with or without Car. (b) Normalized luminescent intensity kinetics of samples in (a) upon 808 nm laser irradiation with a power density of 1.82 W/cm^2. (c) Bright field, upconversion luminescent field, and merged images of IR806-sensitized nanosystems with or without Car in B16-F10 cells. Scale bar, 100 μm. The parts circled by red dotted lines in the merged images are the location of the excitation spots. (d) Normalized luminescent intensity kinetics of samples in (c) under 808 nm laser irradiation with a power density of 1.2×10^3 W/cm^2. Normalization was

performed to the integrated intensity of the green upconversion emission at 540 nm. Data were fitted by the exponential functions.

Conclusions

We investigated here the photophysical and photochemical pathways to uncover the photobleaching mechanism of IR806. Upon excitation, $^1O_2$ is generated via the energy transfer from excited IR806 to triplet oxygen. And then the conjugated carbon chain of IR806 is oxidatively cleaved by the produced $^1O_2$, causing photobleaching. Triplet dynamics of UCNPs-anchored IR806 interactive with triplet oxygen were uncovered for the first time. After coupling to the surface of UCNPs, the triplet dynamics of IR806 are accelerated. Hence, more $^1O_2$ is generated, expediting the photooxidative cleavage of IR806.

Based on this mechanistic study, we introduced a simple and universal method to scavenge the generated $^1O_2$ via Car, effectively inhibiting the photobleaching both in organic and water-soluble solutions. However, the inhibition effect is still limited, perhaps due to the fact that a portion of the generated $^1O_2$ molecules react with IR806 *in situ* but do not diffuse to Car. Hence, we think the chemical crosslinking of Car (or Car analogs) on the structure of IR806 could scavenge $^1O_2$ *in situ* and inhibit photobleaching more effectively. This work demonstrates the photobleaching mechanism of NIR dyes clearly and would help to design strategies to inhibit the photobleaching of organic dye-related nanosystems.

ASSOCIATED CONTENT

Supporting Information

The following files are available free of charge.

AUTHOR INFORMATION
Corresponding Author

*Dr. Guanying Chen: chenguanying@hit.edu.cn

Author Contributions

& These authors contributed equally to this work.

ACKNOWLEDGMENT

This research was supported by the National Natural Science Foundation of China (51972084 and 52272270), Zhejiang Provincial Natural Science Foundation of China under Grant No. LQ23B050006, and China Postdoctoral Science Foundation (2022M722821). This work was also supported in part by U.S. National Institutes of Health award R01NS096317 (B.E.C.). Work at the Molecular Foundry was supported by the Office of Science, Office of Basic Energy Sciences, of the U.S. Department of Energy under Contract No. DE-AC02-05CH11231.

Notes

The authors declare no competing financial interest.

REFERENCES

1. Wang X, Zhang X, Huang D, et al. High-sensitivity sensing of divalent copper ions at the single upconversion nanoparticle level[J]. Analytical Chemistry, 2021, 93(34): 11686-11691.

2. Rafique R, Kailasa S K, Park T J. Recent advances of upconversion nanoparticles in theranostics and bioimaging applications[J]. TrAC Trends in Analytical Chemistry, 2019, 120: 115646.

3. Liang G, Wang H, Shi H, et al. Recent progress in the development of upconversion nanomaterials in bioimaging and disease treatment[J]. Journal of Nanobiotechnology, 2020, 18: 1-22.

4. Li Y, Chen C, Liu F, et al. Engineered lanthanide-doped upconversion nanoparticles for biosensing and bioimaging application[J]. Microchimica Acta, 2022, 189(3): 109.

5. Arai M S, de Camargo A S S. Exploring the use of upconversion nanoparticles in chemical and biological sensors: from surface modifications to point-of-care devices[J]. Nanoscale Advances, 2021, 3(18): 5135-5165.

6. Han S, Sung W, Kim T Y, et al. Upconversion nanoparticles coated organic photovoltaics for near infrared light controlled drug delivery systems[J]. Nano Energy, 2021, 81: 105650.

7. Patel M, Meenu M, Pandey J K, et al. Recent development in upconversion nanoparticles and their application in optogenetics: A review[J]. Journal of Rare Earths, 2022, 40(6): 847-861.

8. Suo H, Zhu Q, Zhang X, et al. High-security anti-counterfeiting through upconversion luminescence[J]. Materials Today Physics, 2021, 21: 100520.

9. Zou W, Visser C, Maduro J A, et al. Broadband dye-sensitized upconversion of near-infrared light[J]. Nature Photonics, 2012, 6(8): 560-564.

10. Wang X, Valiev R R, Ohulchanskyy T Y, et al. Dye-sensitized lanthanide-doped upconversion nanoparticles[J]. Chemical Society Reviews, 2017, 46(14): 4150-4167.

11. Lu D, Cho S K, Ahn S, et al. Plasmon enhancement mechanism for the upconversion processes in $NaYF_4$:Yb^{3+},Er^{3+} nanoparticles: Maxwell versus Forster[J]. ACS nano, 2014, 8(8): 7780-7792.

12. Dong J, Gao W, Han Q, et al. Plasmon-enhanced upconversion photoluminescence: Mechanism and application[J]. Reviews in Physics, 2019, 4: 100026.

13. Nie Z, Ke X, Li D, et al. $NaYF_4$:Yb,Er,Nd@$NaYF_4$:Nd upconversion nanocrystals capped with Mn: TiO_2 for 808 nm NIR-triggered photocatalytic applications[J]. The Journal of Physical Chemistry C, 2019, 123(37): 22959-22970.

14. Chen G, Damasco J, Qiu H, et al. Energy-cascaded upconversion in an organic dye-sensitized core/shell fluoride nanocrystal[J]. Nano letters, 2015, 15(11): 7400-7407.

15. Garfield D J, Borys N J, Hamed S M, et al. Enrichment of molecular antenna triplets amplifies upconverting nanoparticle emission[J]. Nature Photonics, 2018, 12(7): 402-407.

16. Chen G, Shao W, Valiev R R, et al. Efficient broadband upconversion of near-infrared light in dye-sensitized core/shell nanocrystals[J]. Advanced Optical Materials, 2016, 4(11): 1760-1766.

17. Bao G, Wen S, Wang W, et al. Enhancing hybrid upconversion nanosystems via synergistic effects of moiety engineered NIR dyes[J]. Nano Letters, 2021, 21(23): 9862-9868.

18. Engel E, Schraml R, Maisch T, et al. Light-induced decomposition of indocyanine green[J]. Investigative ophthalmology & visual science, 2008, 49(5): 1777-1783.

19. Kaur M, Mandl G A, Maurizio S L, et al. On the photostability and luminescence of dye-sensitized upconverting nanoparticles using modified IR820 dyes[J]. Nanoscale Advances, 2022, 4(2): 608-618.

20. Shibu S, Sugino S, Ono K, et al. Singlet-oxygen-sensitizing near-infrared-fluorescent multimodal nanoparticles[J]. Angewandte Chemie International Edition, 2013, 52: 10559-10563.

21. Khan AU, Kasha M. Direct spectroscopic observation of singlet oxygen emission at 1268 nm excited by sensitizing dyes of biological interest in liquid solution[J]. Proceedings of the National Academy of Sciences, 1979, 76(12): 6047-6049.

22. Nani R R, Kelley J A, Ivanic J, et al. Reactive species involved in the regioselective photooxidation of heptamethine cyanines[J]. Chemical science, 2015, 6(11): 6556-6563.

23. Schweitzer C, Schmidt R. Physical mechanisms of generation and deactivation of singlet oxygen[J]. Chemical reviews, 2003, 103(5): 1685-1758.

24. Toutchkine A, Kraynov V, Hahn K. Solvent-sensitive dyes to report protein conformational changes in living cells[J]. Journal of the American Chemical Society, 2003, 125(14): 4132-4145.

25. Lin C W, Bachilo S M, Weisman R B. Delayed fluorescence from carbon nanotubes through singlet oxygen-sensitized triplet excitons[J]. Journal of the American Chemical Society, 2020, 142(50): 21189-21196.

26. Han S, Deng R, Gu Q, et al. Lanthanide-doped inorganic nanoparticles turn molecular triplet excitons bright[J]. Nature, 2020, 587(7835): 594-599.

27. Zhang J Y, Chen S, Wang P, et al. $NaYbF_4$ nanoparticles as near infrared light excited inorganic photosensitizers for deep penetration in photodynamic therapy[J]. Nanoscale, 2017, 9(8): 2706-2710.

28. Khorobrykh S A, Karonen M, Tyystjärvi E. Experimental evidence suggesting that H_2O_2 is produced within the thylakoid membrane in a reaction between plastoquinol and singlet oxygen[J]. FEBS letters, 2015, 589(6): 779-786.

29. Alexander G, Martin S. Harnessing cyanine photooxidation: from slowing photobleaching to near-IR uncaging[J], Current Opinion in Chemical Biology, 2016, 33: 117-125.

30. NAGANO T, ARAKANE K, Ryu A, et al. Comparison of singlet oxygen production efficiency of C_{60} with other photosensitizers, based on 1268 nm emission[J]. Chemical and pharmaceutical bulletin, 1994, 42(11): 2291-2294.